Tuning laser-induced terahertz spin currents from torque- to conduction-electron-mediated transport

Pilar Jiménez-Cavero[1,2,3,4,5,*], Oliver Gueckstock[1,2,*], Lukáš Nádvorník[1,2,6,†], Irene Lucas[3,4,5], Tom S. Seifert[1,2], Martin Wolf[2], Reza Rouzegar[1,2], Piet W. Brouwer[1], Sven Becker[7], Gerhard Jakob[7], Mathias Kläui[7], Chenyang Guo[8,9], Caihua Wan[8], Xiufeng Han[8,9], Zuanming Jin[10,11], Hui Zhao[12], Di Wu[12], Luis Morellón[3,4.5], Tobias Kampfrath[1,2,†]

1. *Department of Physics, Freie Universität Berlin, Arnimallee 14, 14195 Berlin, Germany*
2. *Department of Physical Chemistry, Fritz Haber Institute of the Max Planck Society, Faradayweg 4-6, 14195 Berlin, Germany*
3. *Instituto de Nanociencia de Aragón (INA), Universidad de Zaragoza, Mariano Esquillor, Edificio I+D, 50018 Zaragoza, Spain*
4. *Departamento Física de la Materia Condensada, Universidad de Zaragoza, Pedro Cerbuna 12, 50009 Zaragoza, Spain*
5. *Instituto de Ciencia de Materiales de Aragón (ICMA). Universidad de Zaragoza CSIC, 50009 Zaragoza, Spain.*
6. *Faculty of Mathematics and Physics, Charles University, Ke Karlovu 3, 12116 Prague, Czech Republic*
7. *Institut für Physik, Johannes Gutenberg-Universität Mainz, 55128 Mainz, Germany*
8. *Beijing National Laboratory for Condensed Matter Physics, Institute of Physics, University of Chinese Academy of Sciences, Chinese Academy of Sciences, Beijing 100190, China*
9. *Center of Materials Science and Optoelectronics Engineering, University of Chinese Academy of Sciences, Beijing 100049, China*
10. *Shanghai Key Lab of Modern Optical Systems, University of Shanghai for Science and Technology, Shanghai 200093, China*
11. *Department of Physics, Shanghai University, Shanghai 200444, China*
12. *Department of Physics and National Laboratory of Solid State Microstructures, Nanjing University, 210093, China*

[*] contributed equally to this work

[†] E-mail: nadvornik@karlov.mff.cuni.cz, tobias.kampfrath@fu-berlin.de

Spin transport is crucial for future spintronic devices operating at bandwidths up to the terahertz (THz) range. In F|N thin-film stacks of a ferro/ferrimagnetic layer F and a normal-metal layer N, spin transport is mediated by (1) spin-polarized conduction electrons and/or (2) torque between electron spins. To identify a cross-over from (1) to (2), we study laser-driven spin currents in F|Pt stacks where F is made of model materials with different degrees of electrical conductivity. For the magnetic insulators YIG, GIG and γ-Fe_2O_3, identical dynamics is observed. It arises from the THz interfacial spin Seebeck effect (SSE), is fully determined by the relaxation of the electrons in the metal layer and provides estimates of the spin-mixing conductance of the γ-Fe_2O_3/Pt interface. Remarkably, in the half-metallic ferrimagnet Fe_3O_4 (magnetite), our measurements reveal two spin-current components with opposite sign. The slower, positive component exhibits SSE dynamics and is assigned to torque-type magnon excitation of the A, B spin sublattices of Fe_3O_4. The faster, negative component arises from the pyro-spintronic effect and can consistently be assigned to ultrafast demagnetization of e-sublattice minority-spin hopping electrons. This observation supports the magneto-electronic model of Fe_3O_4. Our results provide a new route to the separation of torque- and conduction-electron-mediated spin currents.

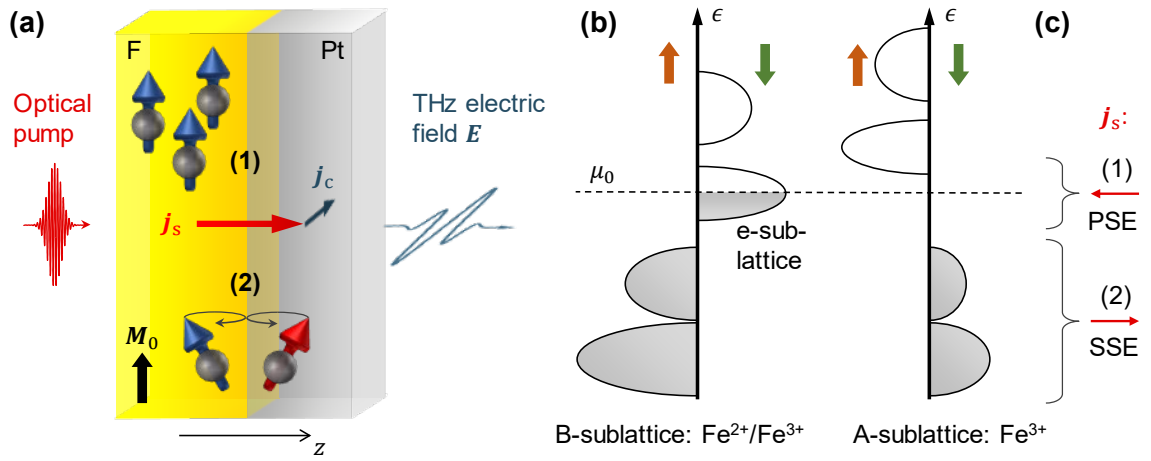

FIG. 1. (a) Schematic of photoinduced spin transport in an F|Pt stack, where F is a magnetic layer with equilibrium magnetization $\boldsymbol{M}_0$, and Pt is platinum. An ultrashort laser pulse excites the sample and induces an ultrafast spin current with density j_s from F to Pt along z. In the Pt, j_s is converted into a transverse charge current with density j_c that gives rise to the emission of a terahertz (THz) electromagnetic pulse. Schematics (1) and (2) indicate spin transfer across the F/Pt interface that is mediated by (1) spin-polarized conduction electrons and (2) spin torque, the latter coupling to magnons in F. (b) Simplified schematic of the single-electron density of states vs electron energy ϵ of the tetrahedral A- and octahedral B-sites of the ferrimagnetic half-metal Fe_3O_4. The DC conductivity predominantly arises from the B-site minority-type hopping electrons (e-sublattice). (c) In our interpretation, optical excitation of the Fe_3O_4|Pt stack triggers spin transfer through both the spin Seebeck effect (SSE) and pyro-spintronic effect (PSE). While the SSE current is mediated by torque between Pt and Fe_3O_4 electron spins far below the Fermi level μ_0 [(2) in panel (a)], the PSE transiently increases the chemical potential of the B-site minority-spin electrons around μ_0 and, thus, induces a conduction-electron spin current [(1) in panel (a)].

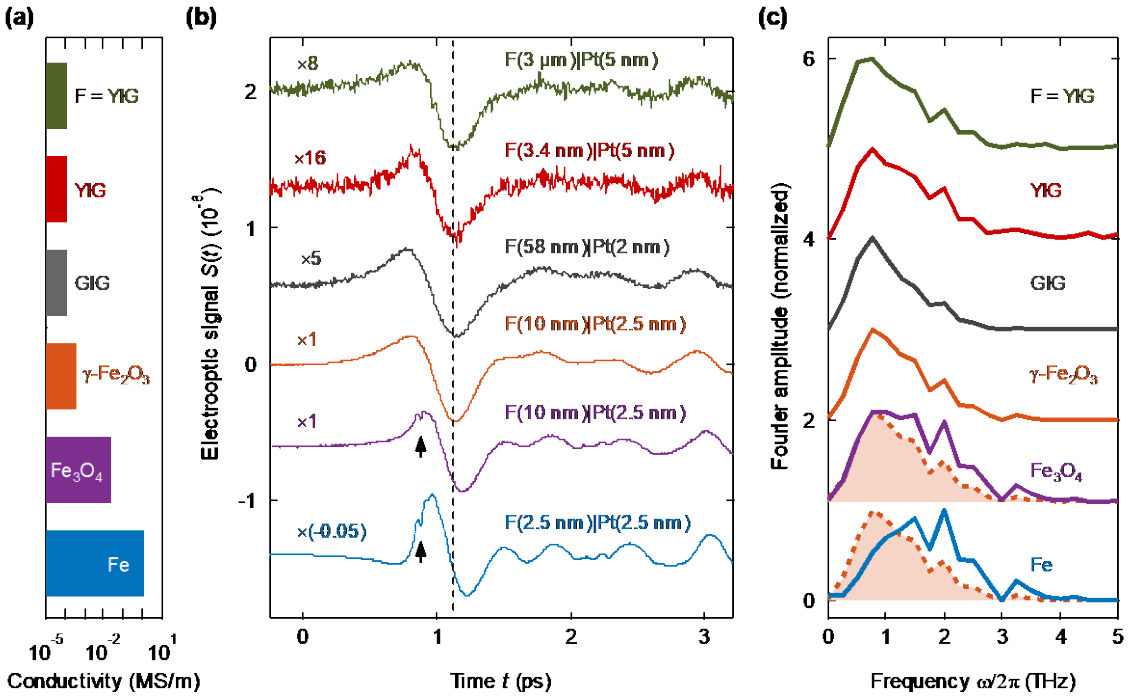

FIG. 2. THz emission from F|Pt bilayers as a function of F-layer conductivity. (a) Electrical conductivities of the studied F materials on a logarithmic scale. (b) Electro-optic signals of THz pulses emitted from various F|Pt bilayers with F=YIG (thick and thin), GIG, γ-Fe_2O_3, Fe_3O_4 and Fe. Note the different amplitude scalings. The time-axis origin is the same for all signals and was determined by the signal from the Fe|Pt reference layers (Fig. S1). The dashed vertical line marks the minimum signal of the insulating F materials YIG, GIG and γ-Fe_2O_3. (c) Fourier amplitude spectra of the signals of panel (b) (normalized to peak height 1). Dashed lines show two duplicates of the spectrum of γ-Fe_2O_3|Pt. Curves in (a) and (c) are vertically offset for clarity.

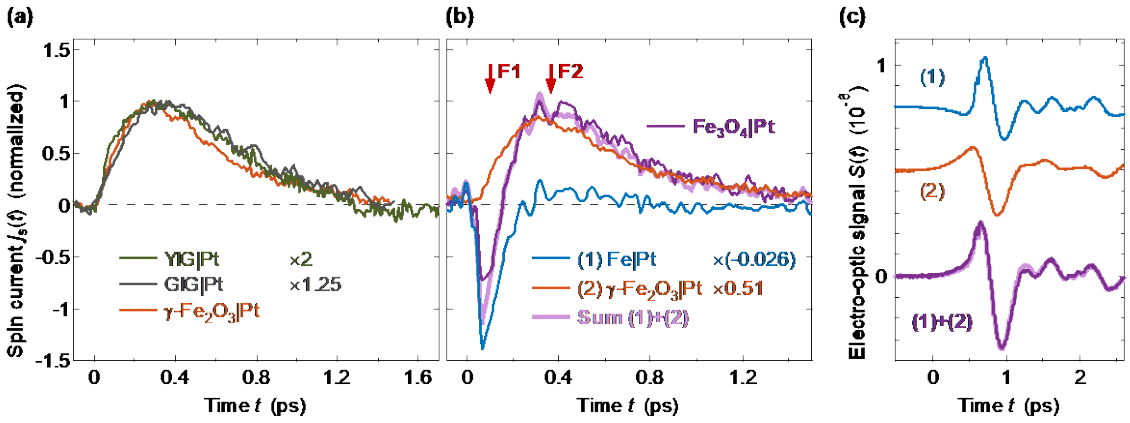

FIG. 3. Ultrafast photoinduced spin currents. (a) Ultrafast spin flow in magnetic-insulator|Pt stacks. Curves show the spin current density in YIG(3 μm)|Pt(5 nm), GIG(58 nm)|Pt(2 nm) and γ-Fe_2O_3(10 nm)|Pt(2.5 nm) as extracted from the THz emission signals of Fig. 2b. Each signal is normalized by the pump-excitation density inside the Pt layer and by the factor in parenthesis. (b) Ultrafast spin flow $j_s(t)$ in Fe_3O_4(10 nm)|Pt(2.5 nm) along with scaled spin currents in γ-Fe_2O_3|Pt and Fe|Pt. The red arrows F1 and F2 mark characteristic features of the spin-current evolution. Note that the $j_s(t)$ of Fe_3O_4|Pt can be well described as a linear combination of the other two spin currents (light-violet curve). (c) Same as in panel (b), but for the THz raw signals.

Introduction. Control over spin currents is a cornerstone of spintronic technologies [1]. New functionalities in such diverse fields as energy conversion and information technologies are envisaged to benefit from the generation, processing and detection of spin currents [2-5]. An important goal is to push the bandwidth of spintronic operations to the terahertz (THz) frequency range, corresponding to ultrafast time scales [1].

A model system for the investigation of the transport of spin angular momentum is the F|N thin-film stack of Fig. 1a, where spin information can be transmitted from a ferro- or ferrimagnetic layer (F) to an adjacent non-ferro/ferrimagnetic metal layer (N). The spin current in F is mediated not only by (1) spin-polarized conduction electrons, which typically dominate spin transfer in metals, but also by (2) magnons, i.e., torque between coupled spins [6,7], which is the main transport channel in insulators. Accordingly, spin transfer across an F/N interface can be mediated by (1) spin-polarized conduction electrons traversing the interface [see (1) in Fig. 1a] and by (2) spin torque between adjacent F and N regions [(2) in Fig. 1a]. As mechanism (2) results in the excitation of magnons in F [8], it can be considered as magnonic spin transfer.

In general, to drive an incoherent spin current of density j_s from F to N, a difference in temperature or chemical potential between the two layers is required [9,10]. For example, for a temperature gradient between F and N, the resulting spin current arises from the interfacial spin-dependent Seebeck effect (SDSE) [11] for channel (1) or the interfacial spin Seebeck effect (SSE) [12-16] for channel (2). In any case, the spin flow from F to N can be detected by conversion of the longitudinal j_s into a transverse charge current with density j_c (Fig. 1a) and measurement of the resulting voltage. For this purpose, N materials with sufficiently large inverse spin Hall effect (ISHE), for instance Pt, are well suited.

A powerful and ultrafast approach to deposit excess energy in F|N stacks is optical excitation by femtosecond laser pulses (Fig. 1a). Measurement of the ultrafast transverse charge current j_c as a function of time t allows one to resolve elementary relaxation processes such as electron thermalization [8] and electron-spin and electron-phonon equilibration [10], but also delivers insights into spin-to-charge-current conversion [17,18]. For an insulating and pump-transparent F, temperature gradients between F and N (i.e., the SSE) were identified as the dominant driving force of the ultrafast j_s. Interestingly, for metallic F, such temperature differences (i.e., the SDSE) were found to make a minor contribution. Instead, chemical-potential-gradients were identified as the relevant driving force of ultrafast spin transport [10]. More precisely, dynamic heating of F leads to a transient spin accumulation or spin voltage, which quantifies the excess of spin angular momentum in F. This phenomenon, which may be termed pyro-spintronic effect (PSE), induces a spin current across the F/N interface [10,19].

There are important open questions regarding the role of THz SSE and PSE. First, the SSE was so far only observed in F|Pt stacks with F made of yttrium iron garnet (YIG). According to the microscopic model of Ref. [8], the spin-current dynamics should be fully determined by the relaxation dynamics of the Pt electrons, independent of the insulating F-layer material. This quite universal implication remains to be shown. Second, with increasing electrical conductivity of the F material, a cross-over from ultrafast SSE to PSE should occur, which was not yet observed. At the cross-over, both spin transport channels (1) and (2) are operative (Fig. 1a), and disentangling them is crucial to maximize the overall generation efficiency of spin currents. The experimental separation of conduction-electron- and magnon-carried incoherent spin transport is challenging under quasistatic conditions [8,20,21]. However, on femtosecond time scales, SSE and PSE dominate and exhibit different temporal dynamics, as indicated by previous works [8,10]. Thus, a separation of the two effects might be possible.

In this work, we study ultrafast photogenerated spin currents in F|Pt bilayers as a function of various magnetic model F-materials with different degrees of electronic conductivity: The ferrimagnetic insulators maghemite (γ-Fe_2O_3), gadolinium iron garnet ($Gd_3Fe_5O_{12}$, GIG) and YIG (with a thickness

ranging over three orders of magnitude), the ferrimagnetic half-metal magnetite (Fe_3O_4), and, for referencing purposes, the ferromagnetic metal iron (Fe). Our study reveals that the ultrafast dynamics of the SSE is independent of the choice of the magnetic insulator (YIG, GIG, γ-Fe_2O_3), its thickness (3.4 nm-3 µm) and growth method. Remarkably, in the half-metallic ferrimagnet Fe_3O_4, we observe simultaneous signatures of both SSE and PSE, whose ultrafast spin currents counteract each other. The PSE current is much smaller and of opposite sign compared to Fe. We assign the PSE current in Fe_3O_4 to the minority hopping electrons (Fig. 1b).

Experimental setup. To launch an ultrafast spin current, the sample under study is excited with near-infrared femtosecond laser pulses (central wavelength of 800 nm, duration of 10 fs, energy of 1 nJ, repetition rate of 80 MHz) from a Ti:sapphire laser oscillator (see Fig. 1a). Part of the energy of the incident pump pulse is deposited in the electronic system of the Pt layer and, if metallic, F layer. Any induced spin current $j_s(t)$ flowing across the F|Pt interface is partially converted into a transverse charge current $j_c(t)$ in the Pt layer through the ISHE, thereby resulting in the emission of electromagnetic pulses with frequencies extending into the THz range (Fig. 1a). We detect the transient THz electric field by electro-optic sampling in a 1 mm thick ZnTe(110) crystal, resulting in the electrooptic signal $S(t)$.

During the experiments, the in-plane equilibrium magnetization $\boldsymbol{M}_0$ of the sample is saturated by an external magnetic field with (magnitude ≈100 mT). We measure signals for two opposite orientations $\pm\boldsymbol{M}_0$. Because we are only interested in effects odd in the magnetization $\boldsymbol{M}_0$, we focus on the antisymmetric signal $S(t) = [S(t, +\boldsymbol{M}_0) - S(t, -\boldsymbol{M}_0)]/2$. All data are acquired at room temperature in air if not mentioned otherwise.

Material choice. For the F material in our F|Pt stacks, we choose common and spintronically relevant two-lattice ferrimagnets with increasing degree of electric conductivity: (i) insulating YIG (thickness 3.4 nm-3 µm), (ii) insulating $Gd_3Fe_5O_{12}$ (58 nm), (iii) insulating γ-Fe_2O_3 (10 nm) and (iv) the half-metal Fe_3O_4 (10 nm) [22]. For referencing, (v) the ferromagnetic metal Fe (2.5 nm) is chosen. As N material, we choose Pt for all samples due to its large spin Hall angle [23]. The approximate F-material conductivities are summarized in Fig. 2a.

The insulators and the metal Fe are expected to transfer spin angular momentum by, respectively, torque [Fig. 1a, (1)] and conduction electrons [Fig. 1a, (2)]. In this respect, Fe_3O_4 is special because it exhibits both localized and mobile electrons with ordered spins. More precisely, the ferrimagnet Fe_3O_4 is a half-metal since its conductivity is dominated by hopping-type transport of minority electrons. Fe_3O_4 possesses two sublattices A and B of, respectively, localized Fe^{2+}/Fe^{3+} and Fe^{3+} spins, which couple antiferromagnetically [22]. In the magneto-electric model, the spins of the "hopping electrons" are aligned predominantly antiparallel to $\boldsymbol{M}_0$ by exchange interaction with A and B and form the e-sublattice [24]. A highly simplified schematic of the electronic structure of Fe_3O_4 is displayed by the spin- and site-resolved single-electron density of states in Fig. 1b [25,26]. The majority (spin-up) electrons exhibit an electronic band gap with a calculated magnitude of 1.7 eV [27], while the presence of minority (spin-down) hopping electrons at the Fermi level μ_0 [24] makes magnetite a half-metal. The measured spin polarization at μ_0 amounts to -72% in Fe_3O_4(001), indicating a nonvanishing number of majority hopping electrons [28].

Sample details. Details on the sample fabrication can be found in the Supplemental Material. In brief, the YIG films are fabricated by three different techniques (pulsed-laser deposition, sputtering and liquid-phase epitaxy). The Fe|Pt reference sample is obtained by growing an Fe layer on top of half the F|Pt region for most of the samples (Fig. S1). The THz emission signal from the resulting F|Pt|Fe regions is dominated by Pt|Fe and equals the reversed signal from an Fe|Pt layer [8]. By means of the Fe|Pt reference signals, the time axes of the THz signals from all samples can be synchronized with an accuracy better than 10 fs.

The pump electric field is approximately constant along z (Fig. 1a) throughout the thin-film stack of our samples. Therefore, the locally absorbed pump-pulse energy is only proportional to $\mathrm{Im}(n^2)$, where n is the complex-valued refractive index of the material at the pump wavelength (800 nm). While the Pt and Fe layers are strongly absorbing ($\mathrm{Im}(n^2)$ =28 and 30) [29], Fe_3O_4 is weakly absorbing (2.3) [30], and YIG, GIG and γ-Fe_2O_3 are largely transparent to the pump beam ($\mathrm{Im}(n^2) \lesssim 1.5$) [31,32].

THz signals. Figure 2b shows electro-optic signals $S(t)$ of THz pulses emitted by the Fe|Pt, γ-Fe_2O_3|Pt, Fe_3O_4|Pt, GIG|Pt and the thinnest as well as the thickest YIG|Pt samples. THz signals from all other YIG samples can be found in Fig. S2a. For YIG(3 µm)|Pt(5 nm) [8] and Fe_3O_4|Pt (Fig. S7), we confirmed that the THz signal increases linearly with the pump power. We make two observations in terms of (i) signal shape and (ii) magnitude.

(i) The waveforms from all samples with YIG, GIG and γ-Fe_2O_3 exhibit very similar dynamics (Fig. 2b and Fig. S3). In contrast, the signal for Fe_3O_4 features a steeper initial rise, a sharp notch right before the first maximum (see black arrow) and a subsequent smaller peak. The global minimum is shifted to later times, as indicated by the dashed vertical line. This trend is even more enhanced for Fe|Pt. These observations indicate that different processes occur in the samples as the F-material conductivity increases (Fig. 2a) [22,33-36]. (ii) While the signals from all YIG-based samples have similar strengths (Fig. S2a), the signals from the γ-Fe_2O_3 and Fe_3O_4 samples are nearly one order of magnitude larger. The signal from Fe|Pt is even more than two orders of magnitude larger than from YIG|Pt.

By Fourier transformation of the time-domain signals $S(t)$ (Fig. 2b), the normalized amplitude $|S(\omega)|$ as a function of frequency $\omega/2\pi$ is obtained (Fig. 2c). As expected from the time-domain data (Fig. 2b), the THz signal of the YIG, GIG and γ-Fe_2O_3 samples have approximately the same amplitude spectrum. For Fe_3O_4, a slightly blue-shifted spectrum with an increased bandwidth is found. This trend is more pronounced for the Fe|Pt spectrum.

Spin current for insulating F. We retrieve the spin current from the measured THz signal waveforms as detailed in the Supplemental Material. Figure 3a displays the resulting $j_s(t)$ in γ-Fe_2O_3(10 nm)|Pt(2.5 nm), GIG(58 nm)|Pt(2 nm) and the YIG(3 µm)|Pt(5 nm) samples. We observe that (i) the spin currents in GIG|Pt, γ-Fe_2O_3|Pt and all YIG|Pt samples exhibit very similar temporal dynamics. (ii) The overall amplitude of the spin current in γ-Fe_2O_3|Pt is about one order of magnitude larger than for the YIG samples. Observations (i) and (ii) are fully consistent with the temporal shape and global amplitude of the underlying raw data (see Fig. 2b). They have three important implications.

First, it is remarkable that the optically induced spin currents in F|Pt bilayers proceed with the same dynamics, even though the magnetic layer is made of very different insulators (F=YIG, GIG and γ-Fe_2O_3) and covers, in the case of YIG, three different growth techniques. Note that in these samples, the pump pulse is to the largest extent absorbed by the Pt layer. Therefore, observation (i) confirms the previous notion [8] that the ultrafast dynamics of the optically induced SSE current are solely determined by the relaxation dynamics of the electrons in the Pt layer. More precisely, the instantaneous spin current density was predicted to monitor the instantaneous state of the electronic system of N=Pt [8],

$$j_s(t) = \mathcal{K}\Delta\tilde{T}_e^N(t). \qquad (1)$$

Here, $\mathcal{K}$ is the interfacial spin Seebeck coefficient, and $\Delta\tilde{T}_e^N$ is the increase of a generalized electronic temperature that is also defined out of thermal equilibrium.

Second, finding (i) also implies that the dynamics of the spin current are independent of the YIG thickness, which covers a wide range from 3.4 nm to 3 µm (Fig. S2b). This result supports the notion [8] that the spin current traversing the YIG/Pt interface stems from YIG regions less than a

few nanometers away from the YIG/Pt interface. It is easily understood given that magnons in YIG have a maximum group velocity of about 10 nm/ps [37] and that the majority of the ultrafast spin-current dynamics proceed within less than 1 ps (Fig. 3a).

Third, we observe that the spin current in the γ-Fe_2O_3|Pt sample is about 2 times higher than for the YIG|Pt or GIG|Pt sample. To understand to which this observation is related to the F/Pt interface, we consider Eq. (1) and note that the SSE coefficient $\mathcal{K}$ is proportional to the product $g_r^{\uparrow\downarrow} M_{IF} a^3$ [8]. Here, $g_r^{\uparrow\downarrow}$ is the real part of the spin-mixing conductance of the F/Pt interface, M_{IF} is the interfacial saturation magnetization, and a is the lattice constant of F. To obtain the relative magnitude of $g_r^{\uparrow\downarrow}$, we divide the THz peak signal of each YIG, GIG and γ-Fe_2O_3 sample by the deposited pump energy density, the THz impedance of the sample, and $M_{IF} a^3$, where bulk magnetization values are assumed for M_{IF} [38-40] (see Table S1). We infer that $g_r^{\uparrow\downarrow}$ is very similar in all three materials and has a relative magnitude of 1, 1 and 1.2. Thus, the spin-mixing conductance of the γ-Fe_2O_3/Pt and GIG/Pt interfaces approximately equals that of the YIG/Pt interface [41]. To the best of our knowledge, this value is the first $g_r^{\uparrow\downarrow}$ estimate of GIG/Pt.

Spin current for half-metal Fe_3O_4. Figure 3b displays the spin current $j_s(t)$ flowing from Fe_3O_4 to the Pt layer. We observe two features with different dynamics: (F1) A fast and sharp negative dip (see red arrow F1), followed by (F2) a slower positive feature (red arrow F2) that decays with a time constant of 0.3 ps. As Fe_3O_4 is a half-metal, it is interesting to compare the dynamics in Fe_3O_4|Pt to those in the two F|Pt stacks with the insulator F=γ-Fe_2O_3 and the metal F=Fe (see Fig. 3b). For F=γ-Fe_2O_3, the spin current across the F/Pt interface is mediated by spin torque, whereas for F=Fe, it is predominantly carried by spin-polarized electrons.

Note that the fast feature (F1) is comparable to $j_s(t)$ of Fe|Pt (blue curve), whereas the slower feature (F2) resembles the $j_s(t)$ of γ-Fe_2O_3|Pt (orange curve). As shown in Fig. 3b, we are even able to reproduce the $j_s(t)$ of Fe_3O_4|Pt by a sum of $-0.026 j_s(t)$ of Fe|Pt and $0.51 j_s(t)$ of γ-Fe_2O_3|Pt. We emphasize that such very good agreement is also observed for the corresponding THz electro-optic signals of Fig. 2b, which is shown in Fig. 3c. We checked explicitly that other signal contributions are negligible: magnetic-dipole radiation due to ultrafast demagnetization of Fe_3O_4 (Fig. S4) [10,42] and signals due to Fe contaminations from the Fe reference layer, which would yield a signal similar to that from Fe|Pt (Fig. S5a).

To summarize, the spin current in Fe_3O_4|Pt can be very well represented by the superposition of the spin currents in two very different samples comprising insulating and conducting magnetic materials, respectively. This remarkable observation strongly suggests that the spin current in Fe_3O_4|Pt has contributions from both the PSE, i.e., through spin-polarized electrons, (see (1) in Fig. 1a) and the SSE, i.e., through spin torque and magnons (see (2) in Fig. 1a).

Physical interpretation for Fe_3O_4. We suggest the following scenario to explain this observation. As the pump excites mainly Pt, a temperature difference between Pt electrons and Fe_3O_4 magnons is established, leading to the SSE spin current across the Fe_3O_4/Pt interface [Fig. 1a, (1)]. From the measured spin-current amplitudes (Fig. 3b), we infer that the spin-mixing conductance of the Fe_3O_4/Pt interface is a factor 7.3 larger than that of YIG/Pt (see Table S1), in excellent agreement with literature [41,43,44]. The sign of the current agrees with that of YIG|Pt, suggesting the SSE in Fe_3O_4 is dominated by the A, B sublattices rather than the oppositely magnetized e-sublattice.

The pump also excites the hopping electrons of Fe_3O_4, which are understood to demagnetize with increasing temperature [24,45-47]. Thus, the chemical potential of the e-sublattice spins increases upon heating by the pump pulse (Fig. 1b,c), and the resulting demagnetization proceeds by spin transfer to the crystal lattice and/or the adjacent Pt layer [10]. Remarkably, as the e-lattice spins are predominantly aligned antiparallel to the equilibrium magnetization $\boldsymbol{M}_0$ (Fig. 1b,c), the PSE tends to increase the magnitude of the total magnetization in Fe_3O_4, whereas in Fe, it is decreased. We, thus, interpret the observed opposite sign of the PSE currents in Fe_3O_4|Pt and Fe|Pt (Fig. 2b) as a

hallmark of the quenching of the residual magnetization of the e-sublattice minority hopping electrons in Fe_3O_4.

The much smaller amplitude of the PSE current in Fe_3O_4|Pt than for Fe|Pt can have several reasons. First, the transport of spin-polarized electrons requires charge conservation [48,49] and, thus, an equal back-flow of charges. However, because the Fe_3O_4 spin polarization at the Fermi level is high (-72%) [28], there are less majority states permitting the backflow of spin-unpolarized electrons from Pt to Fe_3O_4. Second, the mobility of the Fe_3O_4 hopping electrons is likely lower than that of the Fe conduction electrons. Third, at room temperature, the magnetization of the e-sublattice is significantly smaller than the total Fe_3O_4 magnetization [24]. The nonvanishing e-sublattice magnetization inferred here suggests that its ferro-to-paramagnetic transition covers a wide temperature range, possibly because of sample imperfections such as impurities [24]. Fourth, Fe_3O_4 exhibits an order of magnitude smaller absorptance than Fe at the wavelength of the pump pulse (see above). This effect may, however, be significantly mitigated by ultrafast heat transport from Pt to the interfacial Fe_3O_4 regions.

The relaxation time of the PSE is approximately given by the electron-spin equilibration time τ_{es}. Figure 3b suggests that the τ_{es} values of Fe_3O_4 and Fe are comparable and of the order of 100 fs. This conclusion is consistent with previous measurements of ultrafast demagnetization of Fe_3O_4, in which an instantaneous drop of the signal was observed directly after optical excitation [50].

It appears that the PSE dynamics does not significantly perturb the slower SSE dynamics, thereby suggesting that the e-sublattice does not excite magnons of the A, B spins to a sizable extent on time scales below 1 ps. Indeed, ultrafast magnetization dynamics of Fe_3O_4 was reported to exhibit a component with a time constant >1 ns [50]. To summarize, we can consistently assign the PSE current in Fe_3O_4 to the demagnetization of the e-sublattice-type minority hopping electrons at the Fermi energy.

Interface sensitivity. The extracted relative values of $g_{\mathrm{r}}^{\uparrow\downarrow}$ need to be taken with caution because $g_{\mathrm{r}}^{\uparrow\downarrow}$, M_{IF} and, thus, the SSE are very sensitive to the F/Pt interface properties and, therefore, to the growth conditions of the F|Pt stack [51]. For instance, as observed for YIG|Pt previously [8], the spin current amplitude may vary by up to a factor of 3 from sample to sample. Different interface properties may also explain the amplitude variations of the THz signals between the various YIG|Pt samples studied here (Fig. S2b). For Fe_3O_4|Pt, the SSE contribution is robustly observed for samples with Pt grown at room temperature. However, when the Pt deposition temperature of Pt is increased to 720 K, the SSE component disappears (Fig. S5b). We assign this effect to Pt-Fe interdiffusion at the interface, which magnetizes Pt in the vicinity of Fe, as reported previously [52,53].

In conclusion, we study ultrafast spin transport in archetypal F|Pt stacks following femtosecond optical excitation. For the ferri/ferromagnetic layer F, model materials with different degrees of electrical conductivity are chosen. For the magnetic insulators YIG, GIG and γ-Fe_2O_3, our results indicate a universal behavior of the SSE on ultrafast time scales: The spin current is solely determined by the relaxation dynamics of the electrons in the metal layer, and it is localized close to the F/Pt interface. In the half-metallic ferrimagnet Fe_3O_4 (magnetite), our measurements reveal two spin-current components, which exhibit opposite sign and PSE- and SSE-type dynamics. The SSE component is assigned to magnon excitation of the A, B spin sublattices [see (2) in Fig. 1a], whereas the PSE component can consistently be assigned to ultrafast demagnetization of e-sublattice minority-spin hopping electrons [(1) in Fig. 1a]. Our results show that measuring heat-driven spin currents faster than their natural sub-picosecond formation time allows one to unambiguously separate SSE and SDSE contributions by their distinct ultrafast dynamics.

The authors acknowledge funding by German Research Foundation through the collaborative research center SFB TRR 227 “Ultrafast spin dynamics” (projects B02 and A05) and the European Union H2020 program through the project CoG TERAMAG/Grant No. 681917.

References

[1] E. Y. Vedmedenko *et al.*, Journal of Physics D: Applied Physics **53** (2020).
[2] J. Sinova and I. Žutić, Nature Materials **11**, 368 (2012).
[3] S. A. Wolf, D. D. Awschalom, R. A. Buhrman, J. M. Daughton, S. Von Molnár, M. L. Roukes, A. Y. Chtchelkanova, and D. M. Treger, Science **294**, 1488 (2001).
[4] L. Braun, G. Mussler, A. Hruban, M. Konczykowski, T. Schumann, M. Wolf, M. Münzenberg, L. Perfetti, and T. Kampfrath, Nature Communications **7**, 1 (2016).
[5] K. Vandaele, S. J. Watzman, B. Flebus, A. Prakash, Y. Zheng, S. R. Boona, and J. P. Heremans, Materials Today Physics **1**, 39 (2017).
[6] M. Althammer, Journal of Physics D: Applied Physics **51**, 313001 (2018).
[7] S. R. Boona, R. C. Myers, and J. P. Heremans, Energy Environ. Sci. **7**, 885 (2014).
[8] T. S. Seifert *et al.*, Nature Communications **9**, 1 (2018).
[9] G. E. W. Bauer, E. Saitoh, B. J. V. Wees, and P. St, Nature Publishing Group **11**, 391 (2012).
[10] R. Rouzegar *et al.*, arXiv **2103.11710** (2021).
[11] A. Slachter, F. L. Bakker, J. P. Adam, and B. J. Van Wees, Nature Physics **6**, 879 (2010).
[12] K. I. Uchida, H. Adachi, T. Ota, H. Nakayama, S. Maekawa, and E. Saitoh, Applied Physics Letters **97** (2010).
[13] K. Uchida, M. Ishida, T. Kikkawa, A. Kirihara, T. Murakami, and E. Saitoh, Journal of Physics Condensed Matter **26**, 343202 (2014).
[14] R. Ramos *et al.*, Applied Physics Letters **102**, 7 (2013).
[15] J. Xiao, G. E. W. Bauer, K. C. Uchida, E. Saitoh, and S. Maekawa, Physical Review B - Condensed Matter and Materials Physics **81**, 1 (2010).
[16] H. Adachi, K. I. Uchida, E. Saitoh, and S. Maekawa, Reports on Progress in Physics **76** (2013).
[17] O. Gueckstock *et al.*, Adv Mater **33**, e2006281 (2021).
[18] M. Meinert, B. Gliniors, O. Gueckstock, T. S. Seifert, L. Liensberger, M. Weiler, S. Wimmer, H. Ebert, and T. Kampfrath, Physical Review Applied **14** (2020).
[19] A. Fognini, T. U. Michlmayr, A. Vaterlaus, and Y. Acremann, Journal of Physics: Condensed Matter **29**, 214002 (2017).
[20] H. Saglam, W. Zhang, M. B. Jungfleisch, J. Sklenar, J. E. Pearson, J. B. Ketterson, and A. Hoffmann, Physical Review B **94** (2016).
[21] C. M. Jaworski, J. Yang, S. Mack, D. D. Awschalom, J. P. Heremans, and R. C. Myers, Nat Mater **9**, 898 (2010).
[22] J. M. D. Coey, *Magnetism and Magnetic Materials* (Cambridge University Press, 2010).
[23] J. Sinova, S. O. Valenzuela, J. Wunderlich, C. H. Back, and T. Jungwirth, Reviews of Modern Physics **87**, 1213 (2015).
[24] A. R. Muxworthy and E. McClelland, Geophysical Journal International **140**, 101 (2000).
[25] J.-S. Lee, Y.-J. Song, H.-S. Hsu, C.-R. Lin, J.-Y. Huang, and J. Chen, Journal of Alloys and Compounds **790**, 716 (2019).
[26] R. Arras, L. Calmels, and B. Warot-Fonrose, Physical Review B **81** (2010).
[27] H. T. Jeng, G. Y. Guo, and D. J. Huang, Physical Review Letters **93**, 156403 (2004).
[28] W. Wang *et al.*, Physical Review B **87**, 1 (2013).
[29] E. D. Palik, *Handbook of Optical Constants of Solids* (Elsevier Science, 1998), Academic Press handbook series.
[30] A. Schlegel, S. F. Alvarado, and P. Wachter, J. Phys. C Solid State Phys. **12**, 1157 (1979).
[31] S. H. Wemple, S. L. Blank, J. A. Seman, and W. A. Biolsi, Physical Review B **9**, 2134 (1974).
[32] M. R. Querry, edited by C. Report1985).
[33] M. P. Spencer *et al.*, International Journal of Ceramic Engineering & Science **1**, 119 (2019).
[34] M. Fonin, Y. S. Dedkov, R. Pentcheva, U. Rüdiger, and G. Güntherodt, Journal of Physics Condensed Matter **19** (2007).
[35] R. M. Cornell and U. Schwertmann, *The Iron Oxides: Structure, Properties, Reactions, Occurrences and Uses* (Wiley-VCH, Weinheim, 2003), 2nd edn.
[36] N. Thiery *et al.*, Physical Review B **97** (2018).

[37] J. Cramer, T. Seifert, A. Kronenberg, F. Fuhrmann, G. Jakob, M. Jourdan, T. Kampfrath, and M. Klaui, Nano Lett **18**, 1064 (2018).
[38] M. A. Musa, R. a. S. Azis, N. H. Osman, J. Hassan, and T. Zangina, Results in Physics **7**, 1135 (2017).
[39] Aakansha and S. Ravi, Materials Research Express **6** (2020).
[40] P. Jiménez-Cavero *et al.*, APL Materials **5** (2017).
[41] M. Weiler *et al.*, Physical Review Letters **111**, 176601 (2013).
[42] E. Beaurepaire, G. M. Turner, S. M. Harrel, M. C. Beard, J. Y. Bigot, and C. A. Schmuttenmaer, Applied Physics Letters **84**, 3465 (2004).
[43] Z. Qiu, K. Ando, K. Uchida, Y. Kajiwara, R. Takahashi, H. Nakayama, T. An, Y. Fujikawa, and E. Saitoh, Applied Physics Letters **103** (2013).
[44] F. D. Czeschka *et al.*, Phys Rev Lett **107**, 046601 (2011).
[45] K. P. Belov, Physics-Uspekhi **36**, 380 (1993).
[46] K. P. Belov, Physics-Uspekhi **39**, 623 (1996).
[47] K. P. Belov, JETP **36**, 1152 (1996).
[48] A. Hoffmann, physica status solidi (c) **4**, 4236 (2007).
[49] S. Maekawa, S. Valenzuela, E. Saitoh, and T. Kimura, *Spin Current* (Oxford Science Publications, Oxford University Press, 2015).
[50] G. M. Muller *et al.*, Nat Mater **8**, 56 (2009).
[51] T. K. H. Pham *et al.*, Sci Rep **8**, 13907 (2018).
[52] R. Ramos *et al.*, Applied Physics Letters **114** (2019).
[53] H. B. Vasili, M. Gamino, J. Gazquez, F. Sanchez, M. Valvidares, P. Gargiani, E. Pellegrin, and J. Fontcuberta, ACS Appl Mater Interfaces **10**, 12031 (2018).
[54] A. Kehlberger *et al.*, Phys Rev Lett **115**, 096602 (2015).
[55] T. Seifert *et al.*, Spin **7**, 1 (2017).
[56] R. L. Douglass, Physical Review **120**, 1612 (1960).
[57] S. Geprags *et al.*, Nat Commun **7**, 10452 (2016).
[58] C. J. Goss, Phys Chem Minerals **16**, 164 (1988).
[59] J. Noh, O. I. Osman, S. G. Aziz, P. Winget, and J. L. Bredas, Sci Technol Adv Mater **15**, 044202 (2014).
[60] F. N. Shafiee, M. S. Mustaffa, N. H. Abdullah, M. N. Hamidon, I. Ismail, R. Nazlan, I. R. Ibrahim, F. M. Idris, and M. S. E. Shafie, Journal of Materials Science: Materials in Electronics **32**, 10160 (2021).
[61] K. Lal and H. K. Jhans, Journal of Physics C: Solid State Physics **10**, 1315 (1977).
[62] A. M. K. Hofmeister, E. and A. K. Speck, Mon. Not. R. Astron. Soc. **345**, 16 (2003).
[63] B.-W. Dong, L. Baldrati, C. Schneider, T. Niizeki, R. Ramos, A. Ross, J. Cramer, E. Saitoh, and M. Kläui, Applied Physics Letters **114** (2019).